Schemes for ICRF Heating of High-Density Core Plasma in LHD[*]

Kenji SAITO[1,2], Ryosuke SEKI[1,2], Shuji KAMIO[1], Hiroshi KASAHARA[1] and Tetsuo SEKI[1]

[1]*National Institute for Fusion Science, National Institutes of Natural Sciences, Toki, Gifu 509-5292, Japan*
[2]*Department of Fusion Science, The Graduate University for Advanced Studies, SOKENDAI, Toki, Gifu 509-5292, Japan*

Ion Cyclotron Range of Frequencies (ICRF) heating is one of the plasma heating methods in the Large Helical Device (LHD). The wave injected from the ICRF antenna can propagate in the plasma even if the plasma density is extremely high. It was shown that the high power absorption occurs in the plasma core with the second harmonic heating in the case of high-density deuterium plasma in LHD by the calculation with a simple model of the ICRF heating. Wave number perpendicular to the static magnetic field increases with the plasma density, and it enhances the finite Larmor radius effect in the second harmonic heating. Enhanced finite Larmor radius effect and a large amount of resonant ions enable the intense power absorption. By increasing the frequency, the third harmonic heating will also be possible. Though the intensity of the power absorption will decrease, more localized heating on the magnetic axis will be realized because the finite Larmor radius effect works better in the third harmonic heating.

1. Introduction

In the Large Helical Device (LHD) [1, 2], Ion Cyclotron Range of Frequencies (ICRF) heating has been conducted with various frequencies and heating methods, for example, minority ion heating, mode conversion heating, and second harmonic heating [3, 4]. Since the frequency was fixed at 38.47 MHz in 2011 to avoid the risk of breakdown in the transmission line during the operation with lower frequency, the optimization of ICRF heating devices for the high-power and long-pulse operation has been performed. At this frequency, the minority ion heating of hydrogen and the second harmonic heating of deuterium are possible in the standard strength of the magnetic field of 2.75 T at the major radius of 3.6 m. In the campaign of the optimization, the Field-Aligned-Impedance-Transforming (FAIT) antenna with the possible injection power of 1.8 MW per one antenna (15 MW/m^2) was developed [5] and the HAndShake form (HAS) antenna [6] was remodeled by using the technique of the optimization of impedance transformer [7] which was also used in the design of the FAIT antenna.

In LHD, internal diffusion barrier (IDB) [8, 9] was formed by the injection of hydrogen pellets, and this enabled the high-density operation up to the electron density of 1.2×10^{21} m^{-3} at the magnetic axis [1]. With the extreme increase of plasma density, it becomes difficult to inject the neutral beam deeply into the plasma core, and in the Electron Cyclotron Heating (ECH), cutoff emerges and the wave cannot enter into the plasma core region. However, an advantage of ICRF heating is that the wave injected from the ICRF antenna can propagate even if density is very high.

In 2017, the deuterium experiments started in LHD [2]. Therefore, high-density plasma heating of deuterium plasma by the ICRF heating was enabled. An advantage of the second and third harmonic heating compared to the minority ion heating is the core-localized heating due to the finite Larmor radius effect, that is, the enhancement of heating in plasma core region by the finite $k_\perp \rho_s$, where $k_\perp$ is the wave number perpendicular to the magnetic field line and ρ_s is the Larmor radius of a species 's'.

In Section 2, a simple model of heating analysis is introduced. Examples of the simple-model simulation with a comparison to experiments will be shown in Section 3. The simple-model simulations for the second and third harmonic heating in a high-density plasma will be performed in Section 4. The conclusion is provided in Section 5.

2. Simple Model for the Calculation of the Power Absorption

In order to estimate the intensity of the power absorption by the ICRF heating in LHD roughly but easily, a simple-model simulation code was developed in 1999 [3]. The simulation model incorporates the following assumptions:

- Power absorption of fast wave is estimated only in front of the ICRF antennas, that is, in the vertically elongated plasma cross section in LHD.

- Static magnetic field without plasma is used as field data.
- Constant electric field strength $|E|$ is assumed in the region of possible propagation and the electric field in the region of evanescence is assumed to be zero.
- The wave number perpendicular to the magnetic field line and the polarization are calculated with the dispersion relation of hot plasma, where $k_\perp \rho_s$ is approximated to be zero for each species with the given wave number parallel to the magnetic field line $k_{//}$.
- Maxwell distribution is assumed for each species.

This simple model can treat up to three ion-species and also distinguish the heating types such as harmonic number and species. The absorbed power density is calculated with the formulas derived from the antihermitian part of the permittivity tensor of hot plasma. In order to estimate the intensity of the power absorption, the absorbed power density is integrated over the cross section and normalized by $|E|^2$. The spectrum of the antenna current of the HAS antenna is peaked at $k_{//} = 5.6\,\mathrm{m}^{-1}$ in the case of 0-π current phasing assuming the constant current density on the antenna strap. On the other hand, the spectrum of antenna current of the FAIT antenna is broad and peaked at $k_{//} = 0$. In this simulation, $k_{//} = 5\,\mathrm{m}^{-1}$ will be mainly used as a typical $k_{//}$.

3. Examples of Simulations Using the Simple Model

In this section, we introduce two examples of the simple-model simulation to support the above mentioned model.

3.1 Minority ion heating

Figure 1 shows the contour map of the absorbed power density with the cyclotron resonance layers of hydrogen and the flux surfaces on the vertically elongated plasma cross section in the case of the typical minority ion heat-
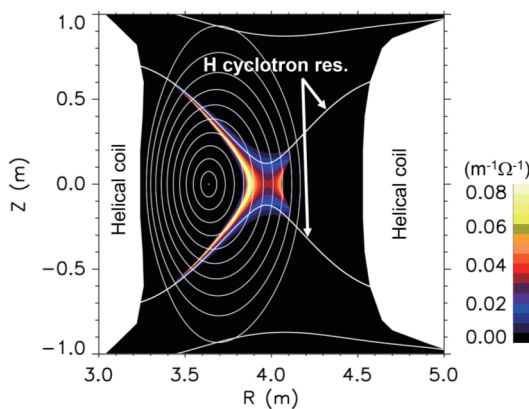

Fig. 1 Contour map of the normalized absorbed power density in the case of the typical minority ion heating.

ing of a plasma consisting of hydrogen and helium. The ICRF antennas are located in between the plasma and the helical coil in the right side of Fig. 1. The magnetic axis is located at the major radius (R) of 3.6 m and the magnetic field strength at the axis (B_0) is 2.75 T. The frequency is 38.47 MHz. The profiles of the ion and electron temperature T_i, T_e and the electron density n_e are given as $T_i = T_e = 2\,\mathrm{keV} \times (1-\rho^2)$ and $n_e = 1 \times 10^{19}\,\mathrm{m}^{-3} \times (1-\rho^8)$, respectively, where the notation ρ is the normalized minor radius. The concentration ratio $n_H/(n_H + n_{He})$ is 0.05 and $k_{//}$ is $5\,\mathrm{m}^{-1}$. The high power density region is shifted slightly from the cyclotron resonance layer to the high field side because the ratio $|E_+|^2/(|E_+|^2 + |E_-|^2)$ is small on the cyclotron resonance layer and the ratio is largest near the left-hand cutoff (L-cutoff) layer which is located in the high field side of the cyclotron resonance layer, where E_+ and E_- are the left-hand and right-hand polarized electric fields, respectively. In this combination of the strength of the magnetic field and the frequency of ICRF heating, the high power absorption region exists widely around the saddle point at $R = 3.97$ m, where the gradient of the magnetic field strength is zero. Then the high normalized total power absorption of $4.92 \times 10^{-3}\,\mathrm{m}/\Omega$ was achieved. The dependency of heating efficiency on the concentration ratio and the best position of the cyclotron resonance layers were well agreed with the experiments in LHD [3].

3.2 Optimized helium-3 heating in H+^{4}He+^{3}He plasma

A new heating scenario using helium-3 was designed as a tool for the core plasma heating of hydrogen rich plasma in LHD by using the simple-model simulation in 2011, though the experiment could not have been carried out in LHD. For the plasma core heating, the frequency was set to 27 MHz. Then, the cyclotron resonance layer of helium-3 almost crosses the magnetic axis at $R = 3.75$ m where the magnetic field strength is 2.64 T. Using a high ion temperature plasma (shot 109947) as a reference, the ion and electron temperature profiles and the electron density profile were given as $T_i = 4.5\,\mathrm{keV} \times (1 - \rho^2)$, $T_e = 3\,\mathrm{keV} \times (1 - \rho^2)$, and $n_e = 1.5 \times 10^{19}\,\mathrm{m}^{-3} \times (1 - \rho^8)$, respectively. By repeating the simulations with changing ratios, the optimized ion ratios, that is, the number of each ion species normalized by the total ion number, were predicted as H: 82.1%, ^{4}He: 17.03%, and ^{3}He: 0.87% in the case of $k_{//} = 5\,\mathrm{m}^{-1}$. Figure 2 (a) shows the cutoff and resonance layers on the vertically elongated plasma cross section in front of ICRF antennas with the obtained optimized concentration ratios, where the dispersion relation of cold plasma was used. It is seen that the cyclotron resonance layer of helium-3 is located in between two L-cutoff layers. These two L-cutoff layers increase $|E_+|$ around the cyclotron resonance layer of helium-3 leading to the enhancement of the power absorption. The region of evanescence between right-side L-cutoff and ion-ion hybrid res-
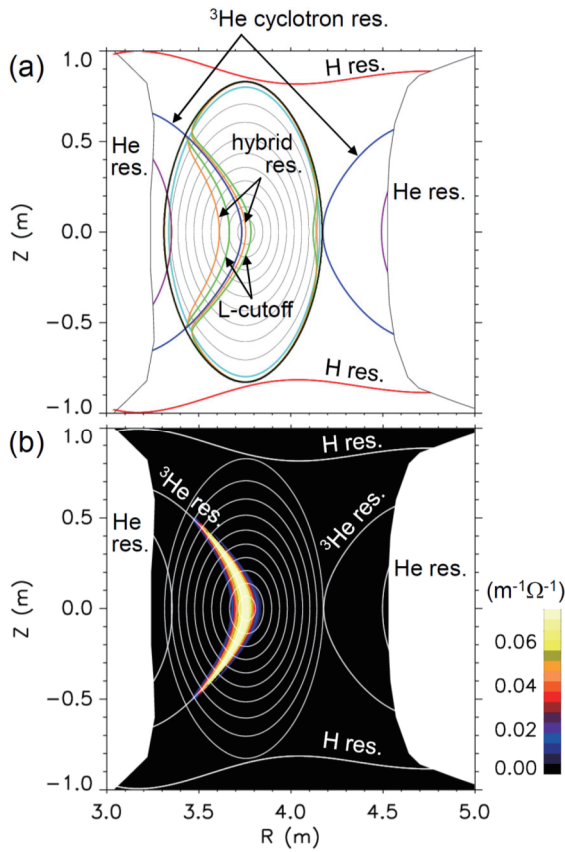
Fig. 2   (a) Cutoff and resonance layers in the optimized helium-3 heating. (b) Contour map of the normalized absorbed power density.
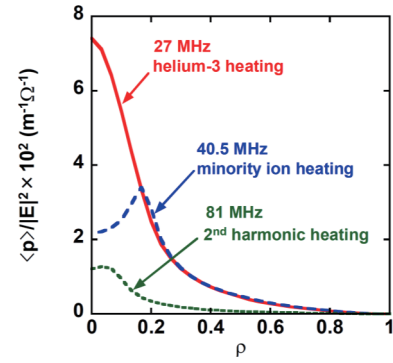

Fig. 3   Comparison of optimized helium-3 heating with other core heating methods. The notation $\langle p \rangle$ is the averaged power density on the flux surface.
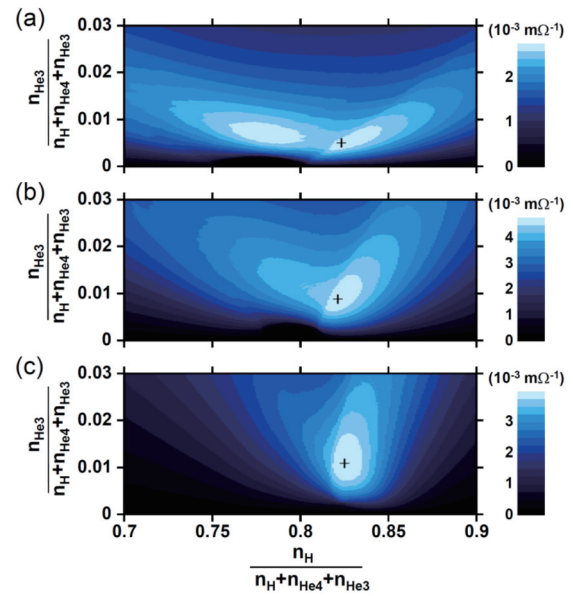

Fig. 4   Scanning of concentration ratios for (a) $k_{//} = 2.5\,\text{m}^{-1}$, (b) $k_{//} = 5.0\,\text{m}^{-1}$, and (c) $k_{//} = 7.5\,\text{m}^{-1}$. Symbol '+' is located at the optimum concentration ratios.

onance layers disappeared in this concentration ratio by the effect of hot plasma. Therefore, the wave from the ICRF antennas can reach the resonance layer of helium-3. Because there are two ion-ion hybrid resonance layers, mode conversion heating may also be enhanced with higher helium-3 concentration ratio, though the simulation is impossible with this simple model. With the above mentioned optimized concentration ratios, the wave power is well absorbed around the resonance layer of helium-3 as shown in Fig. 2 (b). The normalized total power absorption reaches 4.78×10^{-3} m/Ω, which is a similar level to the typical minority ion heating mentioned in Section 3.1. At these concentration ratios, a large tail of helium-3 will be formed owing to a small amount of helium-3 and the large power absorption.

Figure 3 is the comparison with the second harmonic heating of hydrogen plasma and the minority ion heating of H+^{4}He plasma, where the ion and electron temperatures, electron density, and the position of the resonance layer are the same for each heating. Concentration ratio in the minority ion heating is optimized (H: 6.3% and ^{4}He: 93.7%). Peak position in the minority ion heating is slightly off-axis because large $|E_+|$ region is shifted from the magnetic axis to the high field side. The total normalized absorbed power for the second harmonic heating and the minority

ion heating are 6.98×10^{-4} m/Ω and 4.33×10^{-3} m/Ω, respectively. Because the absorbed power of the optimized helium-3 heating is far beyond that of the second harmonic heating and similar to that of the minority ion heating, the helium-3 heating will work as an efficient heating tool.

Figures 4 (a) - (c) show the contour maps of the normalized total absorbed power on H-^{3}He ratios with three values of $k_{//}$. It is found that even if $k_{//}$ varies in the range from 2.5 to 7.5 m^{-1}, the optimized concentration ratios do not change significantly.

The low frequency of 27 MHz leads to the high voltage in the transmission line due to the low loading resistance, which will cause a breakdown at insulators in the transmission line. Further, the cost of helium-3 is extremely high. Therefore, this newly developed optimized helium-3 heating scenario was abandoned in LHD. Soon after that, the frequency of ICRF devices was fixed

at 38.47 MHz for the high-power and long-pulse operation. However, recently, the so-called "three ion-species heating" of H+D+^{3}He plasma was performed successfully with the optimized concentration ratios in tokamaks such as JET ($n_{\mathrm{H}}/n_{\mathrm{e}} \approx 80$ - 82%, $n_{\mathrm{He3}}/n_{\mathrm{e}} \approx 0.1$ - 0.3% [10]) and Alcator C-Mod ($n_{\mathrm{H}}:n_D \approx 70\%:30\%$, $n_{\mathrm{He3}}/n_{\mathrm{e}} \approx 0.5\%$ [10, 11]). The above mentioned optimized concentration ratios of H: 82.1%, ^{4}He: 17.03%, and ^{3}He: 0.87% for LHD correspond to H: 70.15%, D: 29.10%, and ^{3}He: 0.74% and they are close to the experimental concentration ratios. Because the magnetic configuration around the resonance layer of helium-3 crossing the magnetic axis in Figs. 2 (a) and (b) is similar to that of tokamaks, it can be said that the simple-model simulation is useful for predicting heating properties qualitatively.

4. Simulations of the ICRF Heating of High-Density Core Plasma with the Simple-Model Simulation

We applied the above mentioned simple-model simulation to the heating of the high-density IDB plasma. Core heating of extremely high-density plasma will be possible with the ICRF heating because the wave injected from the ICRF antenna can propagate in the high-density region. Moreover, the high-density plasma is a good target for the second and third harmonic heating because the large $k_\perp$ due to the large plasma density improves the heating performance with the finite Larmor radius effect.

4.1 Second harmonic heating

The model plasma is shot 68996 at the time of 1.433 s (see Fig. 1 in Ref. 9), where ion species was hydrogen. The peak of the power deposition profile is located in off-axis region near the normalized minor radius of 0.4 in the case of typical minority ion heating [3]. However, in the model shot, the magnetic axis shifted outward by the Shafranov shift from $R = 3.75$ m to the saddle point of the magnetic field strength at $R = 3.97$ m in the vertically elongated plasma cross section. Therefore, efficient on-axis ICRF heating is enabled. In simulation, the profile of the electron density n_{e} and the ion and electron temperature T_{i}, T_{e} were given as $n_{\mathrm{e}} = n_{\mathrm{e0}}[0.8\exp\{-(\rho/0.35)^{2.5}\}+0.1(1.0 - \rho^{6.5})+0.1]$ and $T_{\mathrm{i}} = T_{\mathrm{e}} = T_0\{1 - (\rho/1.1)^{3.5}\}$, respectively, where $n_{\mathrm{e0}} = 4 \times 10^{20}$ m^{-3} and $T_0 = 1$ keV. Hydrogen used in the model shot was changed to deuterium in the simulation. Wave number parallel to the magnetic field line was set to the typical wave number of 5 m^{-1}. The frequency is 38.47 MHz and the strength of the magnetic field at $R = 3.75$ m was set to 2.616 T so that the cyclotron resonance layers of the second harmonic heating cross the saddle point with this frequency though it was 2.539 T in the model shot. Figure 5 shows the normalized absorbed power density obtained with the simple-model simulation. The normalized total power absorption reaches 3.03×10^{-1} m/Ω, which is more than 60 times that
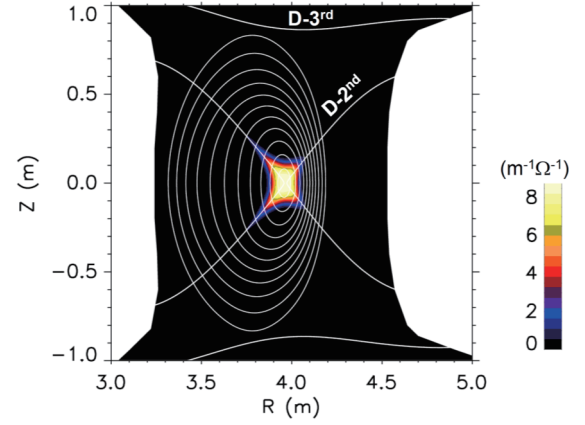

Fig. 5 Contour map of the normalized absorbed power density in the second harmonic heating of the high-density pure deuterium plasma.
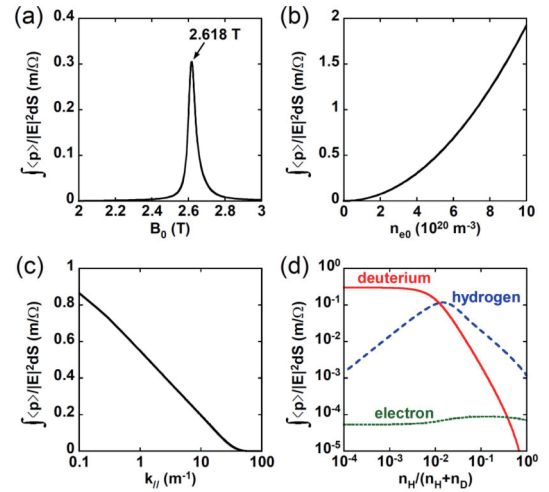

Fig. 6 Scanning of (a) the magnetic field, (b) the electron density, (c) the wave number parallel to the magnetic field, and (d) the concentration ratio of hydrogen. The notation S is the area surrounded by the flux surface at ρ.

of the typical minority ion heating or the optimized helium-3 heating mentioned in Section 3. This high intensity is owing to the large number of resonant particles and the finite Larmor radius effect caused by the large $k_\perp$ in high-density plasma because $k_\perp$ is approximately proportional to the square root of plasma density.

Parameters are scanned as Figs. 6 (a) - (d). In each figure, parameters except for the scanned parameter are fixed at the above mentioned original values. That is, $B_0 = 2.616$ T, $n_{\mathrm{e0}} = 4 \times 10^{20}$ m^{-3}, $k_{//} = 5$ m^{-1}, and $n_{\mathrm{H}}/(n_{\mathrm{H}} + n_D) = 0$. In the scanning of the magnetic field strength shown in Fig. 6 (a), $B_0 = 2.618$ T is the optimum, which is fairly close to the original 2.616 T. As expected, the power absorption increases with the increase of the electron density as shown in Fig. 6 (b). The power absorption decreases with the increase of $k_{//}$ as shown in Fig. 6 (c). The ratio $|E_+|^2/(|E_+|^2 + |E_-|^2)$ is approximately 0.1 on the second

harmonic cyclotron resonance layer in the case of single ion species at the limit of $k_{//} = 0$. Therefore, the Doppler broadening of the resonance region is not necessary for the acceleration of deuterium ions. On the contrary, the deterioration of heating shown in Fig. 6 (c) is due to the Doppler broadening of the resonance region into the lower density and temperature region where the finite Larmor radius effect is weak. Figure 6 (d) shows the dependency of the power absorption on the ratio $n_H/(n_H + n_D)$. Here, we assume that the concentration ratio is uniform in the plasma. The intensity of the second harmonic heating of deuterium decreases with the increase of hydrogen ratio. One reason is the decrease of resonant deuterium ion number. However, the principal reason is due to the decrease of $|E_+|$ around the cyclotron resonance layers because the harmonic number is 1 for hydrogen ions on the cyclotron resonance layers. On the other hand, the intensity of minority ion heating of hydrogen increases with the increase of hydrogen ratio due to the increase of resonant ion number in the region of low hydrogen ratio. As a result, the intensity of the minority ion heating exceeds the intensity of the second harmonic heating. In any concentration ratio, electron heating is weak because of the low electron temperature less than 1 keV. This figure shows if the power absorption is too strong to transmit the power into the magnetic axis, the power absorption can be weakened by adjusting the concentration ratio of hydrogen.

4.2 Third harmonic heating

Figure 7 shows the contour map of the normalized absorbed power density in the case of the third harmonic heating. The frequency was increased to 57.705 MHz, which is 1.5 times the original frequency of 38.47 MHz. The other parameters have the same values used for the calculation of the second harmonic heating shown in Fig. 5. In this case, new ICRF antennas are necessary because the present ICRF antennas are optimized only at the frequency of 38.47 MHz. The total absorbed power normalized by
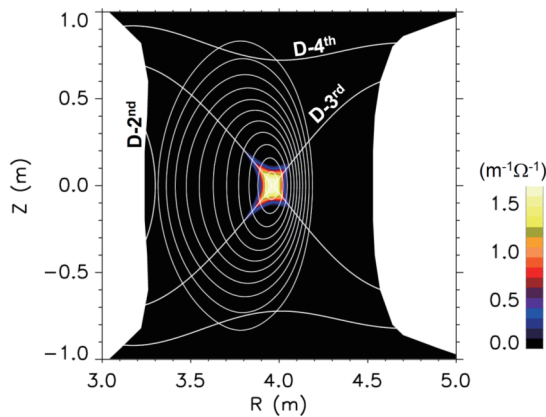
the square of the electric field is 3.96×10^{-2} m/Ω, which is smaller than that of the second harmonic heating. However, the normalized total absorbed power is still more than 8 times that of the typical minority ion heating or the optimized helium-3 heating mentioned in Section 3. The second and fourth harmonic cyclotron resonance layers also exist in edge region. However, the intensity of the power absorption by these resonances is almost zero.

As shown in Fig. 8, the distribution of the power absorption is more core-localized than that of the second harmonic heating because the finite Larmor radius effect works better with higher harmonic heating. In the off-axis region, the power absorption is smaller than that of the typical minority ion heating. Therefore, only the core plasma will be heated.

As shown in Fig. 9, the power absorption by hydrogen ions increases with the ratio $n_H/(n_H + n_D)$ due to the second harmonic heating of hydrogen on the cyclotron resonance layers shown by D-4th in Fig. 7. The power absorption by the third harmonic heating of deuterium does not decrease significantly with the ratio $n_H/(n_H + n_D)$ compared to that by the second harmonic heating of deuterium mentioned in
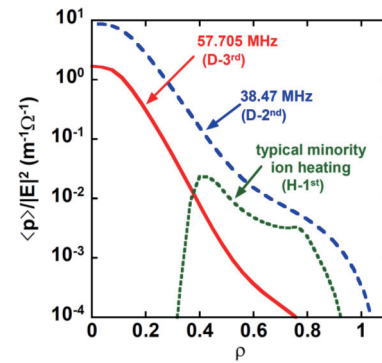
Fig. 8   Power density profiles. Solid line: third harmonic heating (57.705 MHz), Dashed line: second harmonic heating (38.47 MHz), Dotted line: typical minority ion heating (38.47 MHz).

Fig. 7   Contour map of the normalized absorbed power density in the third harmonic heating of the high-density pure deuterium plasma.
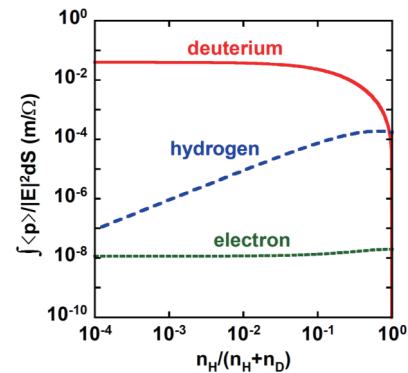
Fig. 9   Dependency of the power absorption on the concentration ratio of hydrogen with the frequency of 57.705 MHz. The parameters except for $n_H/(n_H + n_D)$ were fixed to original values.

Section 4.1.

It is also expected that the enlargement of Larmor radius by the second harmonic heating enhances the third harmonic heating by locating both cyclotron resonance layers at the same position.

5. Conclusion

LHD has advantages in high-density plasma heating, for high-density plasma generation is possible with the formation of IDB and there exist high-performance ICRF heating devices optimized with the frequency of 38.47 MHz. Experiments of the minority ion heating in LHD and the helium-3 heating in tokamaks were well explained with the simple-model simulation. Therefore, it was clarified that the simple-model simulation works as an easy and powerful tool for searching for efficient heating conditions. The simple-model simulation predicts that the high-density plasma will be efficiently heated with the second and third harmonic ICRF heating. In the second harmonic heating of the high-density model plasma, the intensity of the power absorption is more than 60 times that of the typical minority ion heating hitherto performed in LHD or the optimized helium-3 heating designed for the ICRF heating in LHD. With the third harmonic heating, more core-localized heating may be realized, though new ICRF antennas are necessary.

Acknowledgments

[1] Y. Takeiri *et al.*, Nucl. Fusion **57**, 102023 (2017).
[2] T. Morisaki *et al.*, Proc. 27th IAEA Fusion Energy Conference, Gandhinagar, OV/4-2 (2018).
[3] K. Saito *et al.*, Nucl. Fusion **41**, 1021 (2001).
[4] K. Saito *et al.*, Fusion Sci. Technol. **58**, 515 (2010).
[5] K. Saito *et al.*, Fusion Eng. Des. **96-97**, 583 (2015).
[6] H. Kasahara *et al.*, Proc. 38th EPS Conference, Strasbourg, P2.099 (2011).
[7] K. Saito *et al.*, Fusion Eng. Des. **88**, 1025 (2013).
[8] N. Ohyabu *et al.*, Phys. Rev. Lett. **97**, 055002 (2006).
[9] R. Sakamoto *et al.*, Nucl. Fusion **49**, 085002 (2009).
[10] Ye. O. Kazakov *et al.*, Nat. Phys. **13**, 973 (2017).
[11] J.C. Wright *et al.*, Proc. 26th IAEA Fusion Energy Conference, Kyoto, EX/P3-5 (2016).